Chapter 14

Effect Evaluation of Radiative Heat Transfer and Horizontal Wind on Fire Whirlwind

Seigo Sakai

Additional information is available at the end of the chapter

http://dx.doi.org/10.5772/59410

1. Introduction

More than three and a half of years ago, there were a large earthquake in north east area of Japan, i.e. East Japan great earthquake disaster [1], and the residents in the area have been suffering and still on the recovery process from the disaster. A lot of fires were observed in the northeast area of Japan, for example in Kesen-numa City, and so on. Fortunately, there were no reports of fire whirlwinds observed in this disaster, despite of a number of town area fires occurred. However, fire whirlwind is still one of the concerned accidents in the earthquake [2].

A large-scale wide area fire, such as a town area fire or a forest fire, sometimes induces a strong rotating flow, which is to be called fire whirlwind. Fire whirlwind consists of a tornado that includes flames, hot winds and sparks. One of the worst cases which should be avoided at the large-scale fire is the fire whirlwind, because the whirlwind itself is dangerous and play an important role to enhance spread of a fire due to widely scattering sparks.

Even if a small fire occurs, not only a flame induces an upwarding air flow and consumes oxygen from the neighboring, but also a current of air against the flame is present in orde to collect oxygen from wider area. Therefore, a big natural convection will be introduced in the fire current. In the case that the wind may blow from a certain direction into the fire current, uniform air suction collapses with the upwarding air flow. Consequently, a vortex is easily generated, because the fire current turns to a fire whirlwind due to accompanying the upwarding motion with rotating one. Fire whirlwind may be flowed away by a strong downstream wind, or may wander around to collect much oxygen.

There are some experimental works to investigate and reproduce the fire whirlwind in order to explore a flow property and express factors of fire whirlwind outbreaks [3-16]. There are also numerical works in order to analyze the property and the factors [17-24]. In spite that

various factors, such as direction and velocity of horizontal wind or heat generation from the fire, are concerned to outbreak of a fire whirlwind,, it is not sufficient to show outbreak mechanism of a fire whirlwind.

Convective and radiative-convective heat transfer analyses with respect to fire whirlwind were also performed in our laboratory on former studies [25-27], just radiative exchange between solid surfaces was carried out. Therefore, in this study, radiative heat exchange is dealt in consideration of radiative gas using Radiation Element Method by Ray Emission Model (REM^2) [28]. Radiative heat transfer effect on fire whirlwind is discussed.

Then, three dimensional analyses are performed to investigate the thermal and flow fields by using the Finite Volume Method [29] with introducing divergence of radiative heat flux for gas medium. The SIMPLE method is utilized to solve the discretized equations. Natural convection is caused from a plane source of constant temperature in the flat ground. Fire whirlwind is forcely generated stably just above the heat source with introducing air currents from four courners. For making of analysis models, a representative example of the fire whirlwind that occurred at Tokyo in the Great Kanto Earthquake (1923) is referred.

In the analysis, one dimensional radiative exchange analysis above the heat source is compared with three dimensional one to reduce the computational load and time. One-dimensional radiative exchange analysis is suffifient with respect to the accuracy. Then, the composition of participating gases is altered to discuss the effect of radiative heat exchange to the whirlwind flow field. Three dimensional analyses are performed to investigate the thermal and flow fields by using the Finite Volume Method with introducing divergence of radiative heat flux for gas medium. Fire whirlwind is forcely generated stably just above the heat source with introducing air currents from four courners. From the comparison of thermal and flow field between convective flow analysis and combined radiative-convective flow analysis, radiative heat exchange has a great influence to the thermal field and a less influence to the flow field. Increase of participating media concentration gives raise of temperature due to absorption and re-emission, and water vapor influences thermal field more than carbon dioxide.

2. Analysis and modelling

2.1. Radiative exchange

Consider the radiation element of participating medium, which is comprised of a polyhedron surrounded by polygons as shown in Figure 1. The spectral radiation intensity, I_λ, at $\vec{r}$ in the direction $\hat{s}$ can be expressed in terms of the radiation energy balance by

$$\frac{dI_\lambda(\vec{r},\hat{s})}{dS} = -(\kappa_\lambda + \sigma_{s,\lambda}) I_\lambda(\vec{r},\hat{s}) + \kappa_\lambda I_{b,\lambda}(T) + \frac{\sigma_{s,\lambda}}{4\pi}\int_{4\pi} I_\lambda(\vec{r},\hat{s}')\Phi_\lambda(\hat{s}'\to\hat{s})\,d\omega, \quad (1)$$

http://dx.doi.org/10.5772/59410

where κ_λ and $\sigma_{s,\lambda}$ are spectral absorption and scattering coefficients, respectively. Here, S is the path length in the direction $\hat{s}$, $I_{b,\lambda}$ is spectral black-body radiation intensity, $\Phi_\lambda(\hat{s}' \to \hat{s})$ is the phase function from the direction $\hat{s}'$ to $\hat{s}$, and ω is solid angle.

Considering the i-th participating radiation element, and assume that each radiation element has constant uniform temperature of T_i, refractive index and heat generation rate per unit volume, $q_{X,i}$. A ray passing and a part of the ray is scatted. The ray is consisted of absorbed, scattered and transmitted fractions. Additionally, the scattered radiation is assmed to be uniformly distributed over the element. [30]

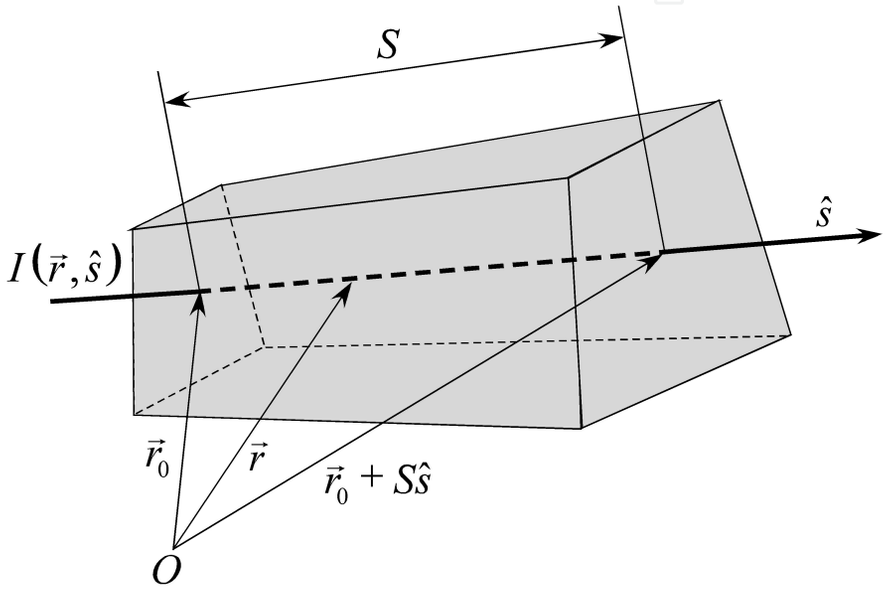

Figure 1. Radiation element

For anisotropic scattering media, an apparent extinction coefficient β_λ^* is introduced, and a corrected scattering albedo Ω_λ^* is obtained by introducing the delta function approximation [31]. Thus, an anisotropic scattering medium can be treated as an isotropic scattering one. The third term on the right hand side of equation (1) can be approximated by

$$\frac{\Omega_\lambda}{2}\int_{-1}^{1} I_\lambda(x,\mu')\Phi_\lambda(\mu')d\mu' \approx \frac{\Omega_\lambda^*}{2}\int_{-1}^{1} I_\lambda(x,\mu')d\mu' \approx \Omega_\lambda^* I_\lambda^D, \tag{2}$$

where Ω_λ is scattering albedo, μ' is directional cosine, and I_λ^D is the average scattered radiant intensity.

A radiation element i can be regarded as either a volume element or a surface boundary. Equation (1) is integrated along the path length $\bar{S}_i(\hat{s}) = V_i / A_i(\hat{s})$ and with respect to all discretized solid angles, in which V_i and $A_i(\hat{s})$ show volume of element and projection area of element

onto the surface normal to $\hat{s}$, respectively [32]. The spectral radiation energy, $Q_{J,i,\lambda}$, from the radiation element i, is given by

$$Q_{J,i,\lambda} = \pi\left(\varepsilon_{i,\lambda} I_{b,i,\lambda} + \Omega_{i,\lambda}^{D} I_{i,\lambda}^{D}\right) A_{i,\lambda}^{R}, \tag{3}$$

where $\varepsilon_{i,\lambda}=1-\Omega_{i,\lambda}^{D}-\Omega_{i,\lambda}^{S}$, in which $\varepsilon_{i,\lambda}$, $\Omega_{i,\lambda}^{D}$ and $\Omega_{i,\lambda}^{S}$ are emissivity, diffuse reflectivity and specular reflectivity of i-th radiation element, respectively. $I_{b,i,\lambda}$ is spectral black-body radiation intensity of i-th radiation element, and $I_{i,\lambda}^{D}$ is average scattered radiant intensity of i-th radiation element. $A_{i,\lambda}^{R}$ is the effective radiation area [28] which is defined as follows,

$$A_{i,\lambda}^{R} \equiv \frac{1}{\pi}\int_{4\pi} A_i(\hat{s})\left[1-\exp\left(-\beta_{i,\lambda}^{*}\bar{S}_i(\hat{s})\right)\right] d\omega. \tag{4}$$

$\beta_{i,\lambda}^{*}$ is apparent extinction coefficient of i-th radiation element. By introducing the absorption view factors $F_{i,j}^{A}$ and the diffuse scattering view factors $F_{i,j}^{D}$ defined by Maruyama [31] and equation (3), the following equations are obtained:

$$Q_{T,i,\lambda} = \pi\varepsilon_{i,\lambda} I_{b,\lambda} A_{i,\lambda}^{R}, \tag{5}$$

$$Q_{J,i,\lambda} = Q_{T,i,\lambda} + \sum_{j=1}^{N} F_{j,i}^{D} Q_{J,j,\lambda}, \tag{6}$$

$$Q_{X,i,\lambda} = Q_{T,i,\lambda} - \sum_{j=1}^{N} F_{j,i}^{A} Q_{J,j,\lambda}. \tag{7}$$

In case of arbitrarily assuming the boundary conditions of the heat transfer rate of the emissive power, $Q_{T,i,\lambda}$, or the net rate of heat generation, $Q_{X,i,\lambda}$ for each radiation element, solving equations (6) and (7) using the method previously described by Maruyama and Aihara [28] gives the unknown $Q_{X,i,\lambda}$ or $Q_{T,i,\lambda}$. The relationship between $q_{X,i}$ and $Q_{X,i,\lambda}$ is obtained by

$$q_{X,i} = \frac{Q_{X,i}}{V_i} = \frac{1}{V_i}\int_0^{\infty} Q_{X,i,\lambda} d\lambda, \tag{8}$$

where λ is wave length. An analytical method for radiative heat transfer, i.e. the radiation element method by ray emission model, REM^2, is used in radiative heat transfer analysis, and the Statistical Narrow Band (SNB) model is combined to the REM^2 to consider the spectral dependence of the radiative properties.

http://dx.doi.org/10.5772/59410

2.2. Thermal and fluid flow fields

The governing equations of thermal and flow fields are the continuum equation, the Navier-Stokes equation, and the energy equation. The thermal and flow fields are assumed to be unsteady state and three dimensional. These equations are normalized and transformed to the following generalized conservation equation.

$$\frac{\partial \phi}{\partial t} + \frac{\partial}{\partial x}(u\phi) + \frac{\partial}{\partial y}(v\phi) + \frac{\partial}{\partial y}(w\phi) = \Gamma\left(\frac{\partial^2 \phi}{\partial x^2} + \frac{\partial^2 \phi}{\partial y^2} + \frac{\partial^2 \phi}{\partial z^2}\right) + S, \tag{9}$$

where t shows time, u, v and w are the normalized velocity components for x, y and z directions, respectively. Variable ϕ takes 1 for the continuum equation, u, v and w for the Navier-Stokes equation, and normalized temperature T for the energy equation. Generalized diffusion coefficient Γ takes 0 for the continuum equation, $1/\mathrm{Re}$ for the Navier-Stokes equation and $1/(\mathrm{Re}\cdot\mathrm{Pr})$ for the energy equation. Normalized source term S takes 0 for the continuum equation, the summation of the normalized pressure term and the normalized buoyancy term by Boussinesq approximation, and the normalized source term from radiative exchange mentioned in the previous section (equation(8)). Turbulent flow is treated by using high Reynolds number turbulence model.

In the thermal and fluid flow analysis, equation (9) is discretized by using the Finite Volume Method [29]. The SIMPLE method is utilized to solve the discretized equations. Physical properties of the mixture are altered depending on the change of temperature.

2.3. Analysis procedure

Figure 2 shows an analysis procedure in this study. Temporal temperature distribution is initially given to analyze nongray radiative heat transfer by REM^2. Then, the derived heat generation rate is introduced to the energy equation, and the thermal and flow field is analyzed by FVM using the SIMPLE method. The derived temperature is introduced to the REM^2 again as an initial temperature distribution, and iteration is repeated until the derived distribution is converged to the initial distribution. Steady state solution is obtained through this iteration loop.

2.4. Analytical model

Figure 3 shows analytical domain for calculation, which scale is based on the Great Kanto Earthquake (1923) in Japan. Heat source on the bottom center has 800m in width and depth, and this value is representative length L. Therefore, the analytical domain is a cubic of 2,000m in width, depth and height. Heat source is applied uniform temperature of 2,000K, and the domain is assumed to be surrounded by circumstance of 293.15K. Initial temperature of the domain is also set to 293.15K. Mixture gas is constituted by water vapor, CO_2 and Nitrogen. All the domain surfaces are assumed to be black for radiative exchange, and the surfaces except the bottom are opened. Fire whirlwind is forcely generated stably just above the heat source

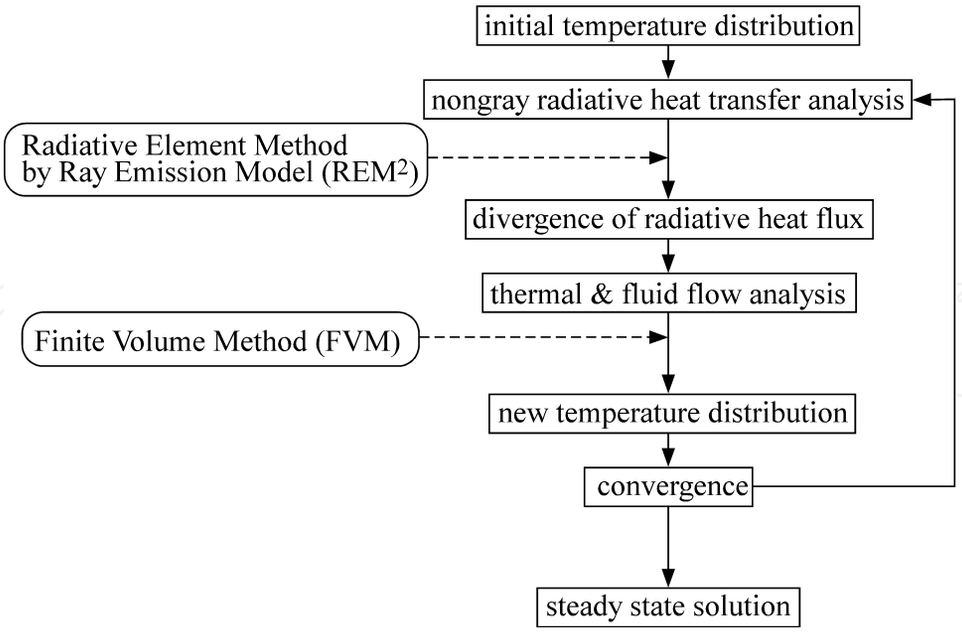

Figure 2. Flow chart of numerical simulation procedure

with introducing air currents from four corners. The currents velocities U are constant of 5m/s at the inlet surfaces of 600m in width and 200m in height. Combustion nor chemical reaction is not considered in the calculation.

Table 1 shows concentration of participating gases in mixture for radiative heat exchange. Carbon dioxide has three values; no concentration, concentration in general atomosphere and the maximum concentration in case of fire. Water vapor also has three values; no concentration, concentrarion of saturated water vapor at the initial temperature and the concentration of saturated water vapor at boiling point.

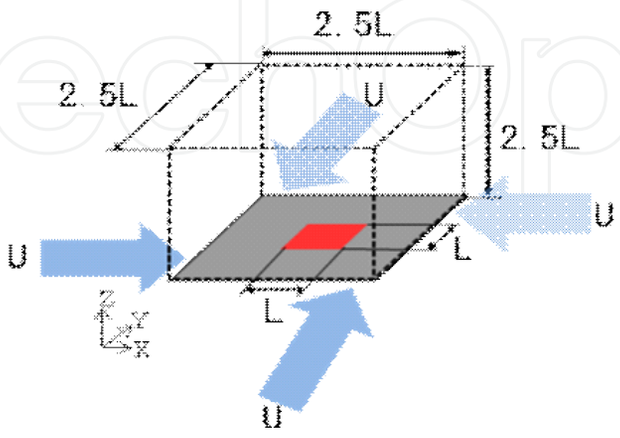

Figure 3. Analytical domain

http://dx.doi.org/10.5772/59410

	Concentration of CO_2 (ppm)	Concentration of H_2O (ppm)
Case A	0	0
Case B	0	3.56×10^4
Case C	3.60×10^2	3.56×10^4
Case D	8.00×10^4	3.56×10^4
Case E	8.00×10^4	1.02×10^6

Table 1. Concentration of participating gases

3. Results and discussions

In this chapter, results are shown and discussed with respect to influence of mesh spacing, effect of radiative exchange, and influence of participating media concentration on heat exchange and flow distribution.

3.1. Influence of mesh spacing on radiative exchabge and flow distribution

Before radiative exchange is coupled with convective flow calculation, influence of mesh spacing on radiative exchange and that on convective flow are individually evaluated.

3.1.1. Convective flow analysis

Figure 4 shows temperature distribution above the heat source by convective flow analysis without considering the radiative heat exchange. Mesh with uniform spacings means uniform spacings for x, y, and z directions, and mech with non-uniform spacings means uniform spacings for x, and y directions and non-uniform spacings for z direction. For all the cases, distributions are almost the same, but the coarse mesh is difficult to simulate the temperature distribution just above the heat source. Mesh with non-uniform spacings is effective to reduce computation load and to keep the accuracy.

Figure 5 shows influence of non-uniform mesh spacings on temperature distribution above the heat source by convective flow analysis without considering the radiative heat exchange. Numbers of uniform mesh spacings for x, and y directions and non-uniform spacings for z direction are increased. For all the cases, distributions are almost the same in case of higher height 400m, but result of the coarse mesh shows lower temperature distribution just above the heat source.

These two figures suggest utilization of at least 30 non-uniform mesh spacings for z direction in the convective flow analysis.

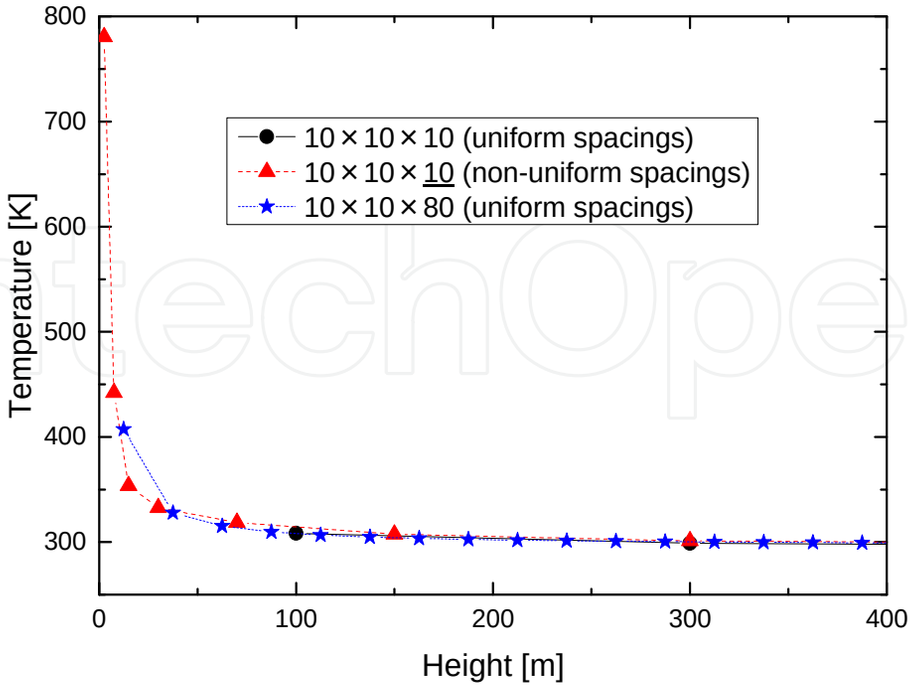

Figure 4. Influence of mesh spacings on convective flow analysis (temperature distribution above the heat source after 30 minutes from air current induction)

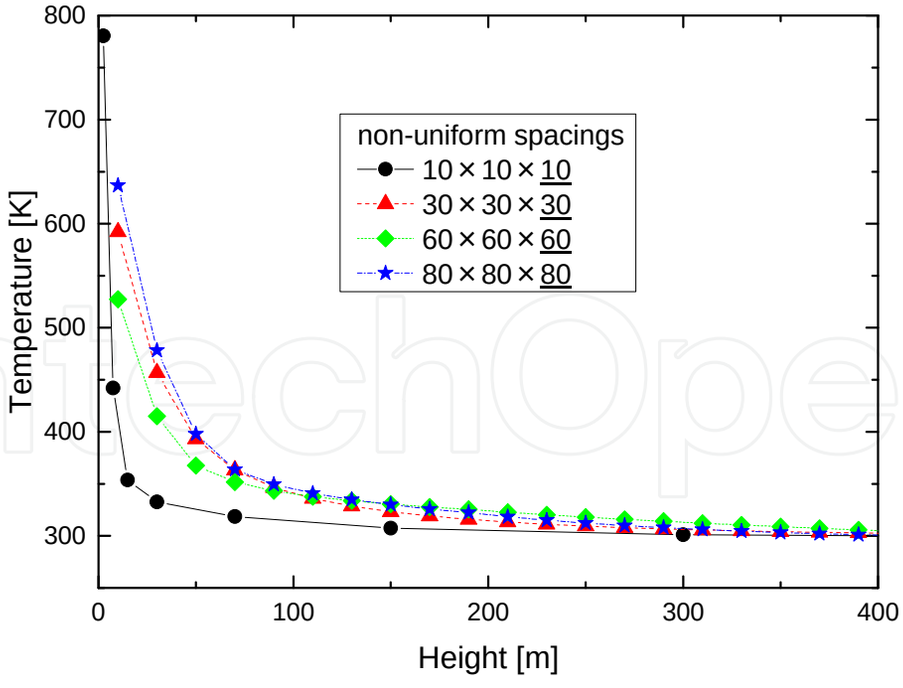

Figure 5. Influence of non-uniform mesh spacings on convective flow analysis (temperature distribution above the heat source after 30 minutes from air current induction)

http://dx.doi.org/10.5772/59410

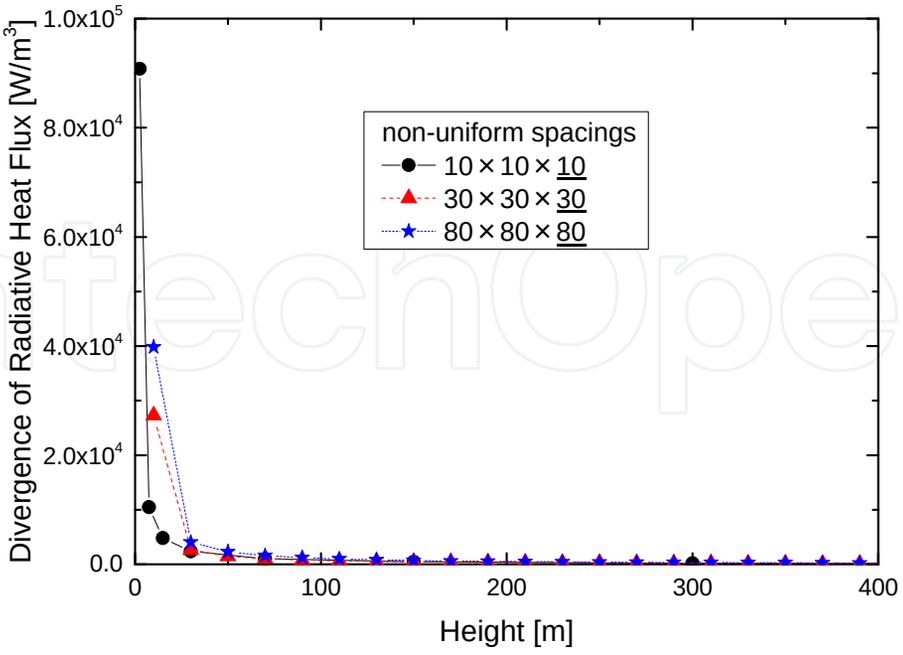

Figure 6. Divergence of radiative heat flux above the heat source after 30 minutes from air current induction

3.1.2. Radiative exchange analysis

Figure 6 shows divergence of radiative heat flux above the heat source. In case of coarse mesh employed, total amount of divergence of radiative heat flux is balanced with higher value just adjacent to the heat source and comparable lower value above the heat source until lower height 100m.

This figure also suggests utilization of at least 30 non-uniform mesh spacings for z direction in the radiative exchange analysis.

3.1.3. Summary

Individual calculation of convective flow analysis and radiative exchange suggest utilization of at least 30 non-uniform mesh spacings for z direction, and 30x30x30 mesh with non-uniform spacings is adapted for combined radiative-convective analysis.

3.2. Effect of radiative heat exchange

In our previous study, scale effect of fire whirlwind is discussed with using the numerical analysis, and relationship between a real phenomenon and the phenomenon in the reduction was examined with considering radiative heat exchange [26]. The P-1 model was utilized to simulate the radiative heat transfer from the heat source at high temperature. It was found that radiative heat exchange played an important role in the heat transfer at the higher temperature field, whereas just radiative exchange between solid surfaces was carried out.

In this study, radiative heat exchange is dealt in consideration of radiative gas using Radiation Element Method by Ray Emission Model (REM^2) [28]. Radiative heat transfer effect on fire whirlwind is discussed.

3.2.1. Comparison of 1-d and 3-d radiative heat exchange

One dimensional radiative exchange analysis above the heat source is compared with three dimensional one to reduce the computational load and time. Figure 7 shows the comparison of divergence of radiative heat flux above the heat source between one dimensional parallel analysis model and three dimensional analysis model. Even though the one dimensional analysis model omitted the effect of surrounding boundaries, these two results coincide comparable. Therefore, further analysis employs one dimensional model for radiative heat exchange.

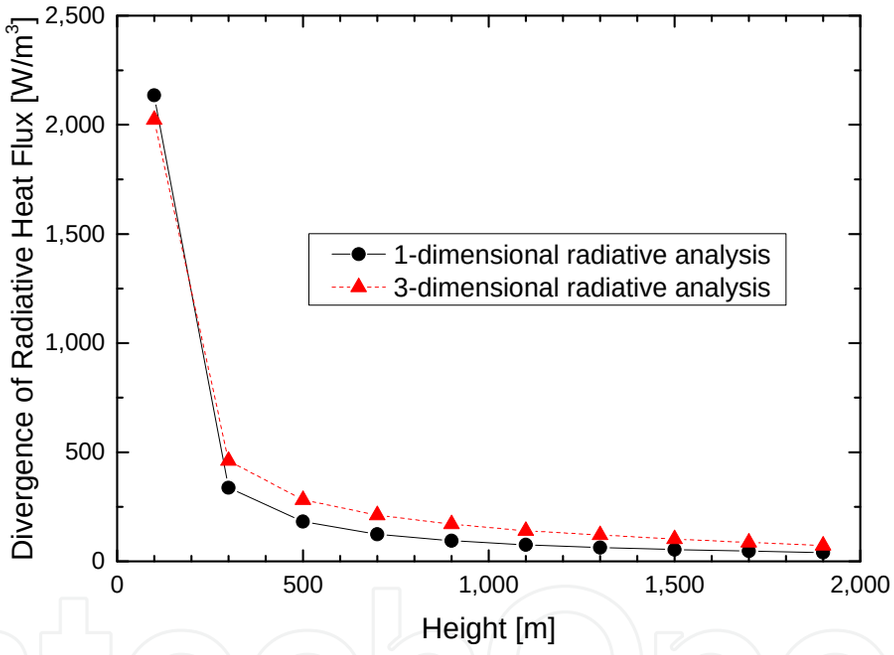

Figure 7. Comparison of 1-d and 3-d radiative analysis (Distribution of divergence of radiative heat flux above the heat source)

3.2.2. Comparison of convective flow analysis and radiative-convective flow analysis

Figure 8 shows heat generation rate for convective flow analysis and divergence of radiative heat flux for radiative heat exchange above the heat source. Though values of divergence of heat flux are smaller than those of heat generation rate, just convective flow analysis ignores these amounts to simulate. It is easily expected that the radiative heat exchange due to participating media plays an important role more than the radiative heat exchange between surfaces.

http://dx.doi.org/10.5772/59410

3.2.2.1. Thermal field

Figure 9 shows comparison of temperature distribution above the heat source after 30 minutes from analysis. As expected from the distribution of heat generation and divergence of radiative heat flux, tempearature distribution is different, especially until lower height 100m. Participating media have much influence to the temperature distribution, and play an important role.

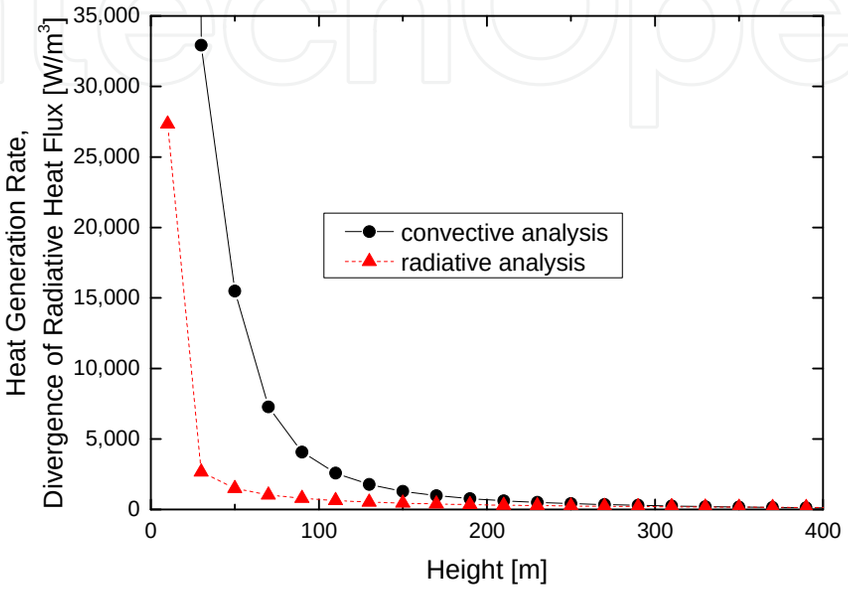

Figure 8. Comparison of heat generation rate and divergence of heat flux above the heat source

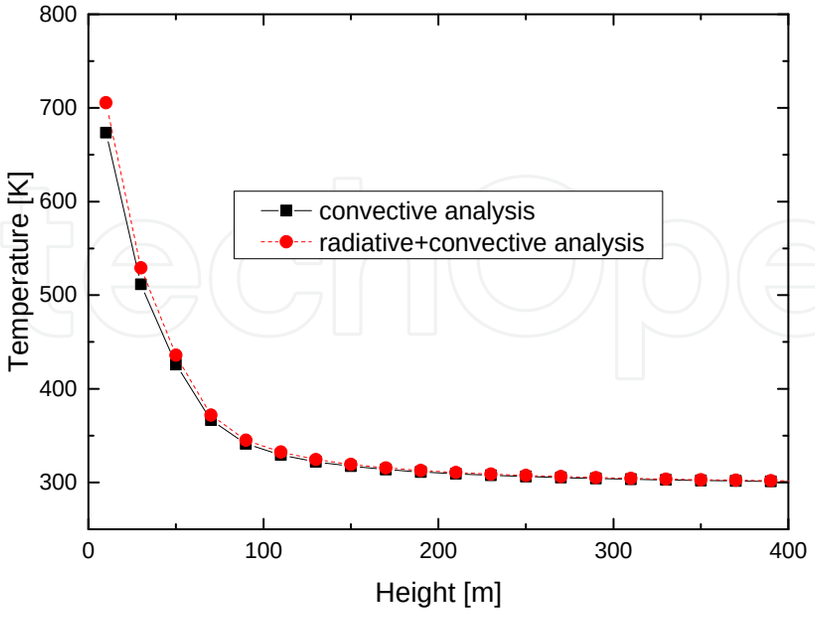

Figure 9. Comparison of temperature distribution above the heat source after 30 minutes from air current induction between convective flow analysis and combined radiative-convective flow analysis

3.2.2.2. Flow field

Figure 10 shows streamlines of the flow field. Lines are colored by velocity magnitude. Whirlwind is stably generated above the heat source, and is shrinked sharply with the height from the heat source.

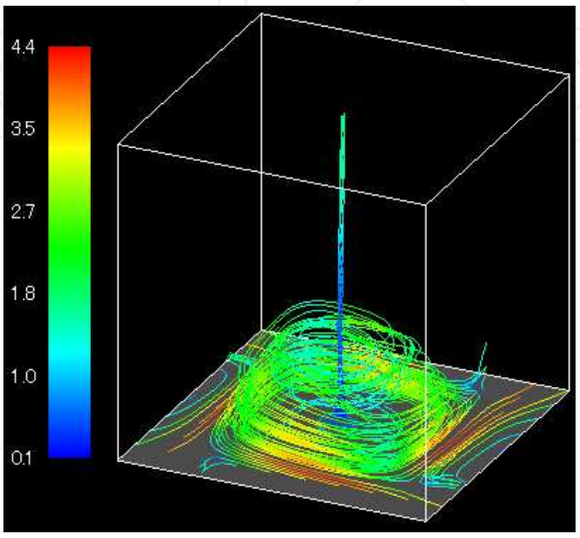

Figure 10. Streamlines of whirlwind

Figure11 shows the upward velocity distribution along the axis from the bottom center. The velocity is almost proportional to the height, and then is toward to a uniform values of about 9 m/s, which is larger than that of inducted air current. Results from the combined radiative-convective flow analysis are almost the same with that from convective analysis.

Figure12 shows the circulation (product of radial distance and circumefential velocity) distribution at the 10m height from the bottom surface. Almost the inner part of whirlwind is assumed to be a forced vortex, and the outer part is to be a free vortex, due to the four air inlets. Results from the combined radiative-convective flow analysis are also almost the same with that from convective analysis.

Figure13 shows the radial position of the maximum circulation for the height, and Figure14 shows the values of the maximum circulation for the height. Figure13 indicates again that the whirlwind is shrinked sharply with the height from the heat source, and Figure14 declares that the maximum circulation is positioned at 100m from the bottom surface due to the friction and 200m height of air current inlet. Results from the combined radiative-convective flow analysis are almost the same with that from convective analysis again.

3.2.2.3. Summary

From the comparison of thermal and flow field between convective flow analysis and combined radiative-convective flow analysis, radiative heat exchange has a great influence to the

http://dx.doi.org/10.5772/59410

thermal field and a less influence to the flow field. Flow field is much characterised by turbulent.

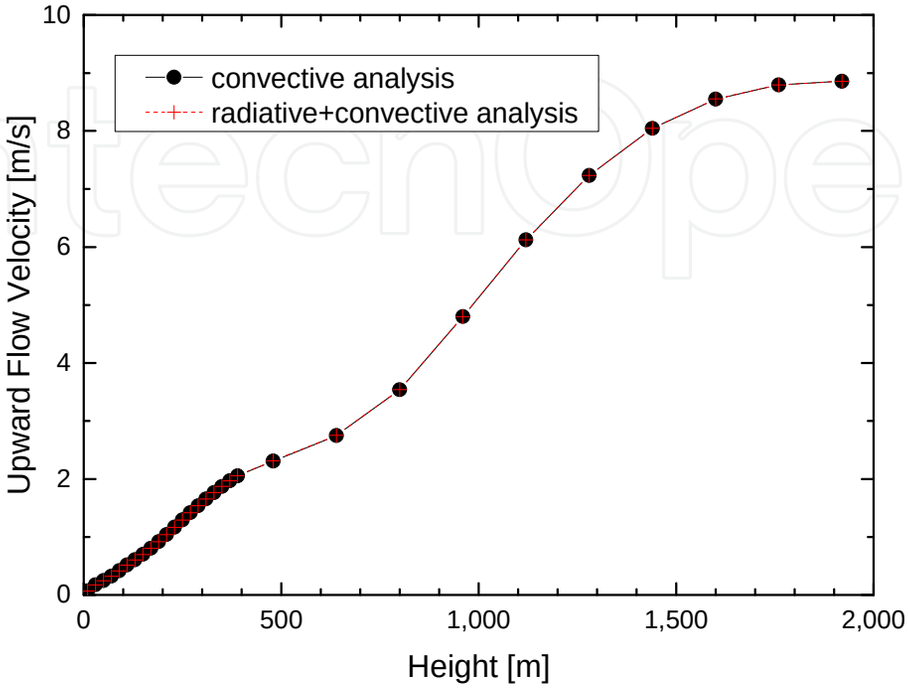

Figure 11. Upward velocity distribution along the axis from the bottom center

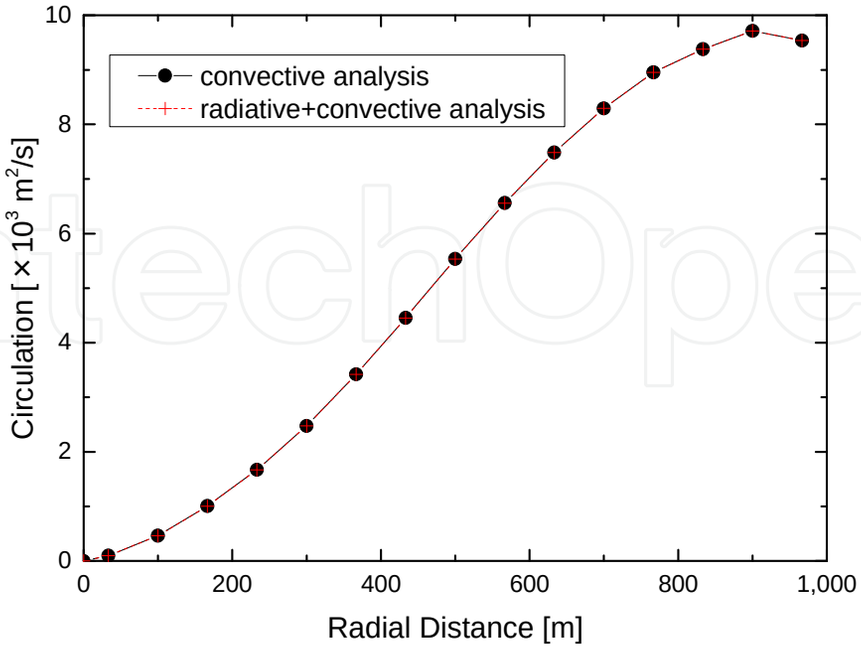

Figure 12. Circulation distribution at the 10m height from the bottom surface

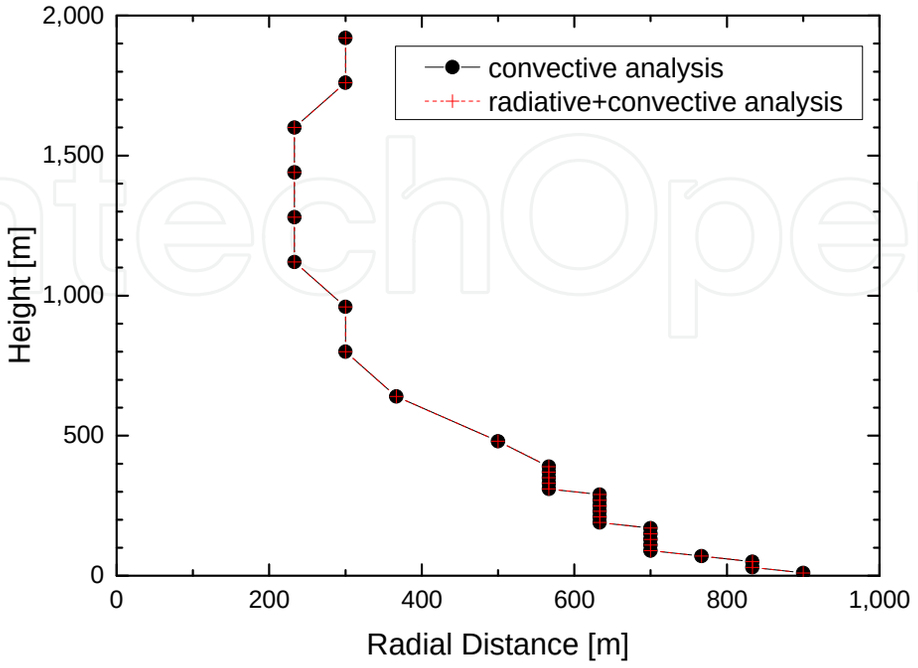

Figure 13. Radial position of the maximum circulation for the height

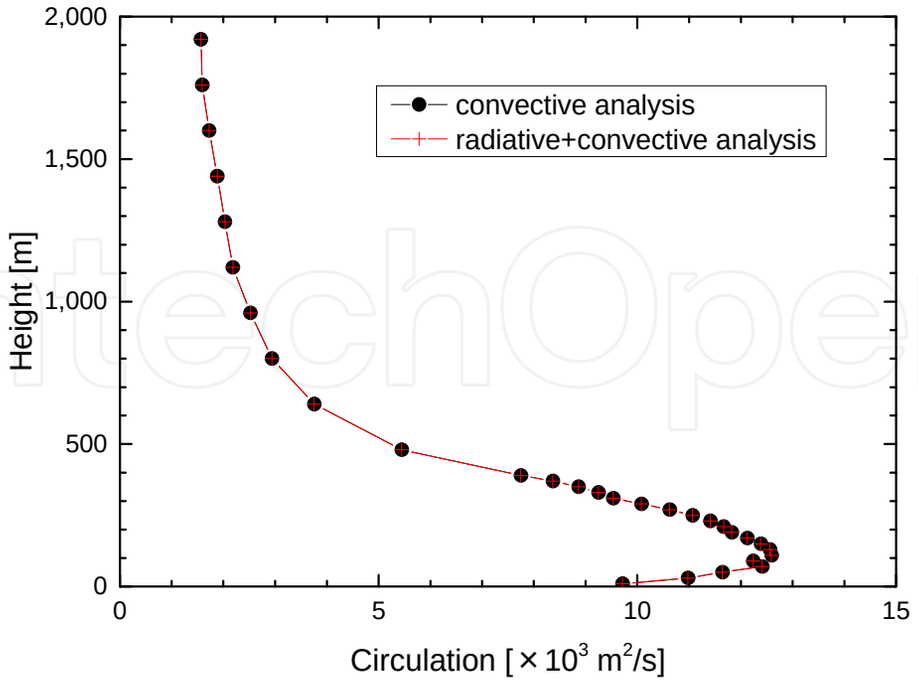

Figure 14. Maximum circulation for the height

http://dx.doi.org/10.5772/59410

3.2.3. Influence of participating media concentration on heat exchange and flow distribution

In practical fire whirlwind, combustion and chemical reaction release some participating media. In this section, representative participating media, i.e. carbon dioxide and water vapor is considered, and the concentration of these participating media is altered to evaluate the influence on heat exchange and flow distribution.

Figure15 shows a comparison of divergence of radiative heat flux with changing the concentration of participating media along the Table 1. Case A means no participating media in the fluid, resulting in no radiative heat exchange. Increase of concentration of participating gases leads the increase of divergence of radiative heat flux in the vicinity of the heat source, i.e. absorption and re-emission of heat due to these participating media. Remarkable increase of divergence of radiative heat flux is observed in case of increase of water vapor concentration.

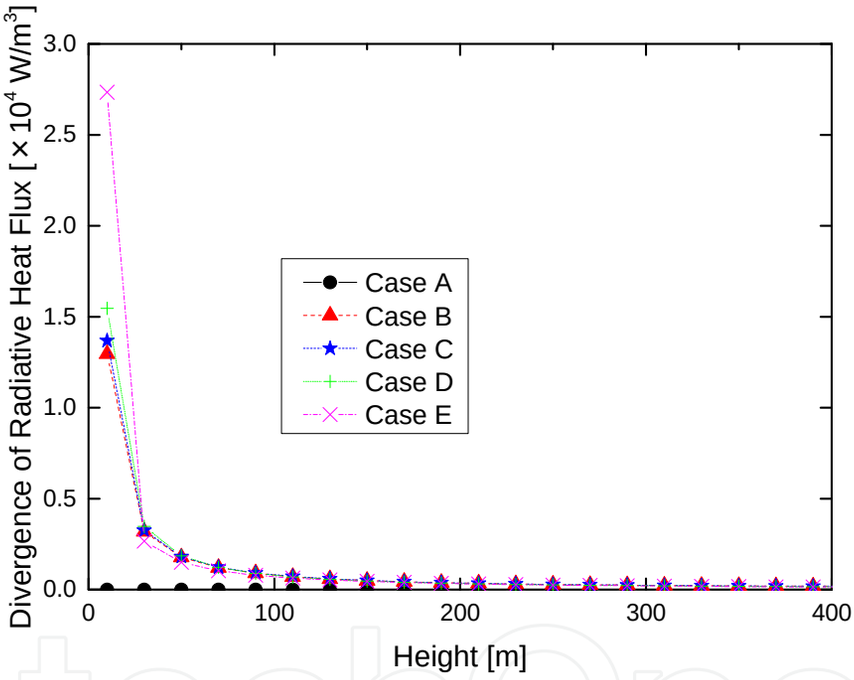

Figure 15. Comparison of divergence of radiative heat flux with changing the concentration of participating media

Figure16 shows a comparison of temperature distribution above the heat source after 30 minutes from air current induction. Increase of divergence of radiative heat flux due to the increase of participating media concentration leads raise of temperature, especially in the vicinity of the heat source.

Figures 17 and 18 shows temperature at the height of 10m from the bottom surface with changing the concentration of carbon dioxide and that of water vapor, respectively. Some values of both participating media concentration are added from the Table 1 for the combined analysis to observe the tendency between temperature and concentration. As discussed in Figure 15, water vapor plays more important role to the thermal field than carbon dioxide.

It is summarized that increase of participating media concentration gives raise of temperature due to absorption and re-emission, and water vapor influences thermal field more than carbon dioxide. However, these calculations employ uniform concentration over the analytical domain. Release and diffusion of participating media have to be considered for more practical evaluation of the whirlwind.

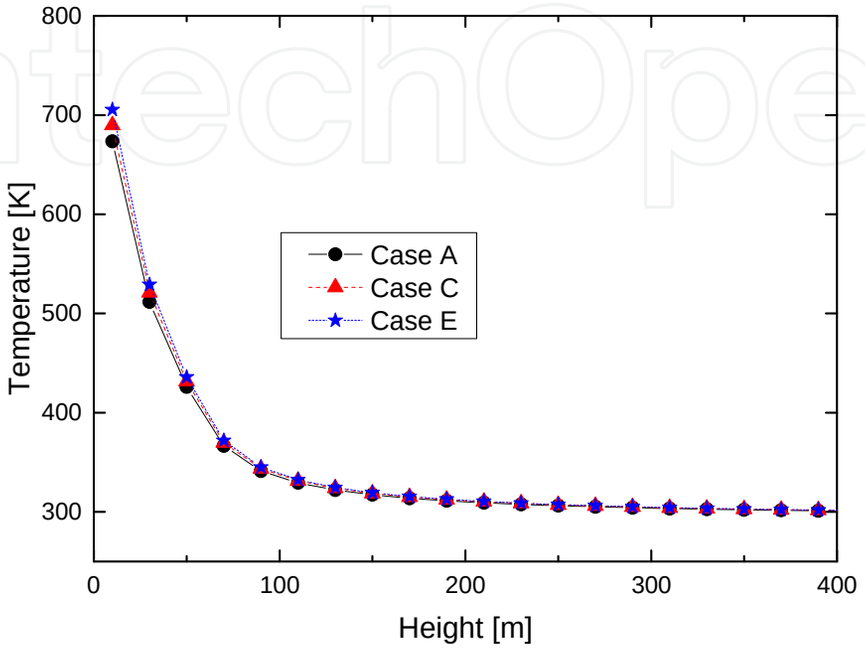

Figure 16. Comparison of temperature distribution with changing the concentration of participating media

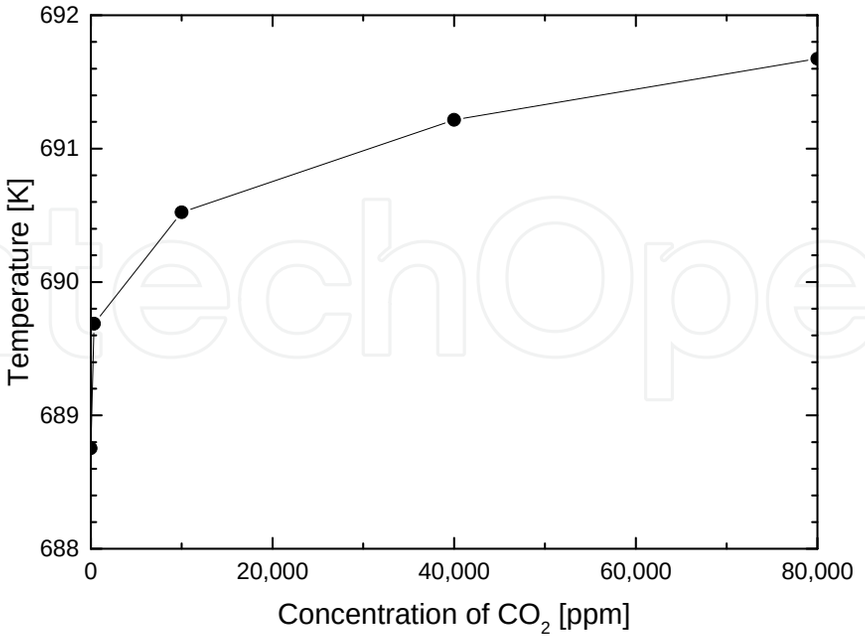

Figure 17. Temperature at the height of 10m from the bottom surface with changing the concentration of carbon dioxide

http://dx.doi.org/10.5772/59410

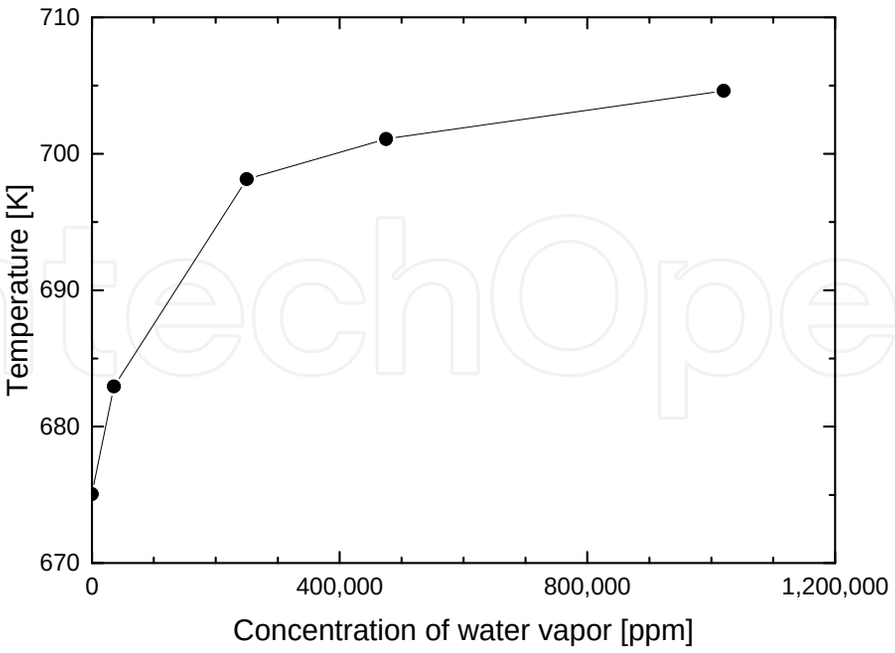

Figure 18. Temperature at the height of 10m from the bottom surface with changing the concentration of water vapor

4. Conclusions

In this study, three dimensional analyses are performed to investigate the thermal and flow fields by using the Finite Volume Method with introducing divergence of radiative heat flux for gas medium. Fire whirlwind is forcely generated stably just above the heat source with introducing air currents from four courners. One dimensional radiative exchange analysis above the heat source is compared with three dimensional one to reduce the computational load and time. One-dimensional radiative exchange analysis is suffifient with respect to the accuracy in these calculations. Then, the composition of participating gases is altered to discuss the effect of radiative heat exchange to the whirlwind flow field. The following concluding remarks are gotten from the combined heat transfer analysis.

- Individual calculation of convective flow analysis and radiative exchange suggest utilization of at least 30 non-uniform mesh spacings for z direction, and 30x30x30 mesh with non-uniform spacings is adapted for combined radiative-convective analysis.
- From the comparison of thermal and flow field between convective flow analysis and combined radiative-convective flow analysis, radiative heat exchange has a great influence to the thermal field and a less influence to the flow field. Flow field is much characterised by turbulent.
- Increase of participating media concentration gives raise of temperature due to absorption and re-emission, and water vapor influences thermal field more than carbon dioxide. However, these calculations employ uniform concentration over the analytical domain.

Release and diffusion of participating media have to be considered for more practical evaluation of the whirlwind.

Nomenclature

$A(\hat{s})$; Area projected onto the surface normal to $\hat{s}$

$A_i(\hat{s})$; Area of i-th radiation element projected onto the surface normal to $\hat{s}$

$A_{i,\lambda}^{R}$; Effective radiation area of i-th radiation element

$F_{i,j}^{A}$; Absorption view factor from i-th radiation element to j-th radiation element

$F_{i,j}^{D}$; Diffuse scattering view factor from i-th radiation element to j-th radiation element

$I_{b,i,\lambda}$; Spectral black-body radiation intensity of i-th radiation element

$I_{b,\lambda}$; Spectral black-body radiation intensity

I_{λ} ; Spectral radiation intensity

$I_{i,\lambda}^{D}$; Average scattered radiant intensity of i-th radiation element

I_{λ}^{D} ; Average scattered radiant intensity

$Q_{J,i,\lambda}$; Spectral radiation energy of i-th radiation element

$Q_{T,i,\lambda}$; Spectral heat transfer rate of the emissive power of i-th radiation element

$Q_{X,i,\lambda}$; Spectral net rate of heat generation of i-th radiation element

$q_{X,i}$; Heat generation rate of i-th radiation element per unit volume

$\vec{r}$; Position vector

$\vec{r}_0$; Position vector

S ; Path length

$\bar{S}_i(\hat{s})$; Path length of i-th radiation element $(\bar{S}_i(\hat{s}) = V_i / A_i(\hat{s}))$

$\hat{s}$; Direction vector

$\hat{s}'$; Direction vector

T ; Temperature

T_i ; Temperature of i-th radiation element

t; Time

u ; Normalized velocity component for x direction

V_i ; Volume of i-th radiation element

v; Normalized velocity component for y direction

w ; Normalized velocity component for z direction

Greek symbols

$\beta^*_{i,\lambda}$; Apparent extinction coefficient of i-th radiation element

β^*_{λ} ; Apparent extinction coefficient

Γ ; Generalized diffusion coefficient

$\varepsilon_{i,\lambda}$; Spectral emissivity of i-th radiation element

κ_{λ} ; Spectral absorption coefficient

λ ; Wave length

μ' ; Directional cosine

$\sigma_{s,\lambda}$; Spectral scattering coefficient

$\Phi_{\lambda}(\hat{s}' \rightarrow \hat{s})$; Phase function from the direction $\hat{s}'$ to $\hat{s}$

ϕ ; Variable for governing equations

$\Omega^D_{i,\lambda}$; Spectral diffuse reflectivity of i-th radiation element

$\Omega^S_{i,\lambda}$; Spectral specular reflectivity of i-th radiation element

Ω_{λ} ; Scattering albedo

Ω^*_{λ} ; Corrected scattering albedo

ω ; Solid angle

Acknowledgements

This work was partially supported by JSPS KAKENHI Grant Number 24560222.

Author details

Seigo Sakai*

Yokohama National University, Japan

References

[1] Takewaki I, Murakami S, Fujita K, Yoshitomi S, Tsuji M. The 2011 off the Pacific coast of Tohoku earthquake and response of high-rise buildings under long-period ground motions. Soil Dynamics and Earthquake Engineering 2011; 31(11) 1511–1528.

[2] Hough S E, Bilham R G. After the Earth Quakes: Elastic Rebound on an Urban Planet, Oxford University Press USA 2005.

[3] Graham H E. Fire whirlwinds. Bulletin American Meteorological Society 1955; 36 99–103.

[4] Emmons H W, Ying S J. The fire whirl. Proceedings of the Combustion Institute 1967; 11 475–488.

[5] Byram G M, Martin R E. The Modeling of Fire Whirlwinds. Forest Science 1970; 16(4) 386-399.

[6] Haines D A, Updike G H. Fire Whirlwind Formation over Flat Terrain. USDA Forest Service Research Paper 1971; NC-71.

[7] Martin R E, Pendleton D W, Burgess W. Effect of Fire Whirlwind Formation on Solid Fuel Burning Rates. Fire Technology 1976; 12(1) 33-40.

[8] Muraszew A, Fedele J B, Kuby W C. The fire whirl phenomenon. Combustion and Flame 1979; 34 29-45.

[9] Emori R I, Saito K. Model experiment of hazardous forest fire whirl. Fire Technology 1982; 18(4) 319-327.

[10] Satoh K, Yang K T. Experimental Observations of Swirling Fires. Proceedings of ASME Heat Transfer Division 1996; HTD-335(4) 393-400.

[11] Hayashi Y, Ohmiya Y, Iwami T, Saga T. Experimental Study on Fire and Plume Properties Using BRI's Fire Wind Tunnel Facility. International Journal for Fire Science and Technology 2003; 22 17-35.

[12] Liu N A. Experimental and Theoretical Investigation on Fire Interactions and the Induced Firewhirls in Square Fire Arrays. Proceedings of Fifth NRIFD International Symposium on Forest Fires, 2005; Tokyo 293-301.

[13] Kuwana K, Sekimoto K, Saito K, Williams F A. Can We Predict the Occurrence of Extreme Fire Whirls? AIAA JOURNAL 2007; 45 16-19.

[14] Liu N A, Liu Q, Deng Z H, Satoh K, Zhu J P. Burn-out Time Data Analysis on Interaction Effects among Multiple Fires in Fire Arrays. Proceedings of the Combustion Institute 2007; 31 2589-2597.

[15] Kuwana K, Sekimoto K, Saito K, Williams F A. Scaling fire whirls. Fire Safety Journal 2008; 43(4) 252-257.

[16] Chuah K H, Kuwana K, Saito K, Williams F A. Inclined fire whirls. Proceedings of the Combuation Institute 2011; 33 2417-2424.

[17] Satoh K, Yang K T. Simulations of swirling fires controlled by channeled self-generated entrainment flows [A]. Fire Safety Sci., Proceedings of the 5th International Symposium[C] 1997; 201-212.

[18] Battaglia F, Rehm R G, Baum H R. Fluid Mechanics of Fire Whirls: An Inviscid Model. Physics of Fluids 2000; 12(11) 2859-2867.

[19] Battaglia F, McGrattan K B, Rehm R G, Baum H R. Simulating Fire Whirls. Combustion Theory and Modelling 2000; 4(3) 123-138.

[20] Snegirev A Y, Marsden J A, Francis J, Makhviladze G M. Numerical studies and experimental observations of whirling flames. International Journal of Heat and Mass Transfer 2004; 47 2523–2539.

[21] Hassan M I, Kuwana K, Saito K, Wang F. Flow Structure Of A Fixed-frame Type Firewhirl. Proceedings of the Eighth International Symposium, International Association for Fire Safety Science, 18-23 September 2005, Beijing, China. 2005; 951-962.

[22] Chuah K H, Kushida G. The prediction of flame heights and flame shapes of small fire whirls. Proceedings of the Combustion Institute 2007; 31 2599–2606.

[23] Grishin A M. Effect of the Interaction between Fire Tornadoes on Their Propagation. Doklady Physics 2007; 52(10) 521-522.

[24] Grishin A M, Matvienko O V, Rudi Y A. Mathematical Modeling of Gas Combustion in A Twisted Jet and of The Formation of A Fiery Whirlwind. Journal of Engineering Physics and Thermophysics 2009; 82(5) 906-913.

[25] Sakai S, Watanabe Y. Numerical Study of Interaction between Natural Convection Flow and horizontal wind. Proceedings of the FEDSM2007, 5th Joint ASME/JSME Fluids Engineering Conference, 30 July – 2 August 2007, San Diego, California, USA. 2007; FEDSM2007-37212.

[26] Sakai S, Miyagi N. Numerical Study of Fire Whirlwind Taking into Account Radiative Heat Transfer, IOP Conference Series: Materials Science and Engineering 2010; 10 012031.

[27] Sakai S. Numerical Prediction of Fire Whirlwind Outbreak and Scale Effect of Whirlwind Behavior. In: Moustafa A. (ed.) Advances in Geotechnical Earthquake Engineering – Soil Liquefaction and Seismic Safety of Dams and Monuments. Rijeka: In Tech; 2012. p383-404.

[28] Maruyama S, Aihara T. Radiation Heat Transfer of Arbitrary Three-Dimensional Absorbing, Emitting and Scattering Media and Specular and Diffuse Surfaces. Trans. ASME, Journal of Heat Transfer 1997; 119 129-136.

[29] Patankar S V. Numerical heat transfer and fluid flow. In: Phillips M A, Millman E M. (ed.) USA: Hemisphere Publishing Corporation; 1980.

[30] Maruyama S, Mori Y, Sakai S. Nongray radiative heat transfer analysis in the anisotropic scattering fog layer subjected to solar irradiation. Journal of Quantitative Spectroscopy and Radiative Transfer 2004; 83 361-375.

[31] Maruyama S. Radiative heat transfer in anisotropic scattering media with specular boundary subjected to collimated irradiation. International Journal of Heat and Mass Transfer 1998; 41 2847-2856.

[32] Nishikawa T, Maruyama S, Sakai S. Radiative Heat Transfer Analysis within Three-Dimensional Clouds Subjected to Solar and Sky Irradiation. Journal of the Atmospheric Sciences 2004; 61 3125-3133.